Optics Letters

Solitons in a $\mathcal{PT}$-symmetric $\chi^{(2)}$ coupler

Magnus Ögren,[1,*] Fatkhulla Kh. Abdullaev,[2] and Vladimir V. Konotop[3]

[1]School of Science and Technology, Örebro University, 701 82 Örebro, Sweden
[2]Physical-Technical Institute, Uzbekistan Academy of Sciences, 100084, Buyuk Ipak Yuli Str., 2-b, Tashkent, Uzbekistan
[3]Centro de Física Teórica e Computacional and Departamento de Física, Faculdade de Ciências, Universidade de Lisboa, Campo Grande 2, Edifício C8, Lisboa 1749-016, Portugal
*Corresponding author: magnus@ogren.se

Received 22 August 2017; revised 12 September 2017; accepted 12 September 2017; posted 13 September 2017 (Doc. ID 305223); published 4 October 2017

We consider the existence and stability of solitons in a $\chi^{(2)}$ coupler. Both the fundamental and second harmonics (SHs) undergo gain in one of the coupler cores and are absorbed in the other one. The gain and loss are balanced, creating a parity-time ($\mathcal{PT}$) symmetric configuration. We present two types of families of $\mathcal{PT}$-symmetric solitons having equal and different profiles of the fundamental and SHs. It is shown that the gain and loss can stabilize solitons. The interaction of stable solitons is shown. In the cascading limit, the model is reduced to the $\mathcal{PT}$-symmetric coupler with effective Kerr-type nonlinearity and the balanced nonlinear gain and loss.

OCIS codes: (130.2790) Guided waves; (350.5500) Propagation.

https://doi.org/10.1364/OL.42.004079

Optical solitons in media with quadratic ($\chi^{(2)}$) nonlinearities have been the subject of intensive investigations over the last few decades, both theoretically and experimentally [1,2]. Several types of quadratic bright soliton solutions have been reported in an exact analytical form [3–6], and families of solutions were investigated numerically [7]. Spatial one-dimensional quadratic solitons in optical waveguides have been observed [8,9].

Direct nontrivial generalization of guiding structures for the $\chi^{(2)}$ solitons [1] towards their manipulations is a $\chi^{(2)}$ coupler. Such a device supports propagation of four different field components, which are two fundamental fields (FFs) and the respective second harmonics (SHs) in each of the two coupler arms. The coupling of the fields in the arms can be implemented in different ways. The simplest model was with the tunnel coupling between FF only, used for investigation of discrete $\chi^{(2)}$ solitons [10]. While carrier wave states and all-optical switching in $\chi^{(2)}$ couplers were the subject of many studies [11], solitons in coupled optical waveguides with quadratic nonlinearities were explored much less. Numerical simulation of propagation of temporal solitons and their switching in the $\chi^{(2)}$ coupler has been performed in [12], while the existence of solitons and their stability for the case of no walk-off and full matching was shown in [13].

In this Letter, we investigate solitons in a $\chi^{(2)}$ coupler with gain in one arm and absorption in another one (as illustrated in Fig. 1). The gain and loss are balanced, thus implementing a parity-time ($\mathcal{PT}$) symmetric [14] system. Motivation of our study resides in peculiarities of such a device. Indeed, in spite of the gain and loss, it allows for propagation of soliton families [15], which depend on one (or several) parameters. Since the gain, usually implemented in a form of active impurities, is controlled by an external pump field, the parameters of solitons can be varied at fixed parameters of the hardware, making the control flexible, and opening possibilities, for instance for novel types of optical switching or nonreciprocal devices. Furthermore, including the gain and loss in the system changes the parameter regions of the existence and stability of $\chi^{(2)}$ solitons. Additionally, the cascading limit of such a coupler gives origin to a $\mathcal{PT}$-symmetric coupled nonlinear Schrödinger equations, of a new type. Recently, exploring different settings it was found [16–18] that the gain and loss modify the matching conditions, making it possible the resonant mode interaction which otherwise is not allowed in the conservative waveguides.

Since four different harmonics are involved, from the theoretical point of view the $\chi^{(2)}$ coupler can be viewed as a particular type of nonlinear $\mathcal{PT}$-symmetric "quadrimer." For the Kerr-type nonlinearity, quadrimers received considerable attention (see e.g., [15] and references therein). In the case of $\chi^{(2)}$ nonlinearity, the previous studies were restricted to stationary (nondiffractive) propagation [19].

We focus on the interaction of waves occurring in coupled active and absorbing planar waveguides (Fig. 1). The equations describing light propagation in such $\chi^{(2)}$ coupler read

$$\begin{aligned} iu_{1,z} &= -u_{1,xx} + \kappa_1 u_2 - 2u_1^* v_1 + i\gamma_1 u_1, \\ iv_{1,z} &= -\frac{1}{2} v_{1,xx} + \kappa_2 v_2 - u_1^2 - q v_1 + i\gamma_2 v_1, \\ iu_{2,z} &= -u_{2,xx} + \kappa_1 u_1 - 2u_2^* v_2 - i\gamma_1 u_2, \\ iv_{2,z} &= -\frac{1}{2} v_{2,xx} + \kappa_2 v_1 - u_2^2 - q v_2 - i\gamma_2 v_2. \end{aligned} \tag{1}$$

Here we use the dimensionless variables [2] $u_j = 2L_d d E_j$ and $v_j = L_d d e^{iqz} E_j$, where $j = 1, 2$ labels the waveguide for the electric field envelopes E_j of the FFs (u_j) and SHs (v_j), the dimensionless propagation distance is $z = Z/2L_d$ and the transverse coordinate is $x = X/\eta$. The linear coupling between harmonics in different arms is $\kappa_i = K_i L_d$, and the mismatch

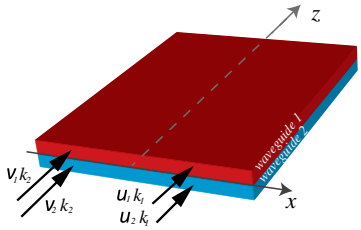

Fig. 1. Schematic presentation of a planar $\chi^{(2)}$ coupler. The first and second waveguides have gain and absorption, respectively. Four beams are applied at the input ($z = 0$).

of the propagation constants is $q = \Delta k L_d$, assumed to be the same in both arms, where $K_{1,2}$ are the physical couplings of FF and SHs (we consider them positive), $d = \omega_1/(\epsilon_0 n_1 c)\chi^{(2)}$ is the parameter of quadratic nonlinearity, $\Delta k = 2k_1 - k_2$ is the phase mismatch, η is the characteristic beam width, and $L_d = k_1\eta^2$ is the linear diffraction length. The strength of the gain in the first waveguide and absorption in the second waveguide are characterized by the parameters $\gamma_j > 0$, for the first ($j = 1$) and second ($j = 2$) harmonics, respectively. The equality of the gain and loss ensures $\mathcal{PT}$-symmetry of the coupler.

The model (1) includes diffraction effects and generalizes the model of the $\mathcal{PT}$-symmetric coupler considered in [19]. On the other hand, inclusion of the gain and loss represents a $\mathcal{PT}$-symmetric generalization of the conservative coupler considered in [13]. We also notice that the system (1) obeys Galilean invariance. Thus, having found localized beams, which we described by the four-component vector $\psi(x, z) = (u_1(x, z), v_1(x, z), u_2(x, z), v_2(x, z))^T$ with T standing for the transpose, and which propagate along the z direction, one readily obtains beams propagating under a nonzero angle θ with respect to the z-axis in the form $(e^{i\varphi}u_1(\xi, z), e^{2i\varphi}v_1(\xi, z), e^{i\varphi}u_2(\xi, z), e^{2i\varphi}v_2(\xi, z))^T$, where $\varphi = wx/2 - w^2 z/4$, $\xi = x - wz$, and $w = \tan\theta$. In the presence of a gain, a necessary condition for the possibility of observing localized nonlinear beams is the stability of the zero solution. This corresponds to the choice of the parameters in the so-called unbroken $\mathcal{PT}$-symmetric phase [14]. Such stability is obtained from the linear dispersion relation. Using the ansatz $u, v \sim e^{ibz+ikx}$ in (1), we obtain four branches of the linear modes:

$$b_{1,2} = -k^2 \pm \sqrt{\kappa_1^2 - \gamma_1^2}, \quad b_{3,4} = -\frac{1}{2}k^2 + q \pm \sqrt{\kappa_2^2 - \gamma_2^2}. \tag{2}$$

Thus, the $\mathcal{PT}$-symmetry is unbroken (real b_j:s) if $\gamma_1 < \kappa_1$ and $\gamma_2 < \kappa_2$. Below we restrict the discussions to these constraints.

Let the parameters satisfy the relation as follows:

$$\kappa_1^2\gamma_2 = 2\kappa_2\gamma_1\sqrt{\kappa_1^2 - \gamma_1^2}. \tag{3}$$

In this case, one can introduce δ through the relations $\sin(\delta) = \gamma_1/\kappa_1$, where $0 \le \delta \le \pi/2$, and define $\beta_1 = \kappa_1\cos(\delta)$, and $\beta_2 = \kappa_2\cos(2\delta)$. Then the system (1) has a solution of the form (by analogy with the ansatz introduced in [20]) $u_1 = u$, $u_2 = \pm e^{\pm i\delta}u$, $v_1 = v$, $v_2 = \pm e^{\pm 2i\delta}v$, where the functions u and v solve the standard system of the $\chi^{(2)}$ equations:

$$\begin{aligned} iu_z &= -u_{xx} + \beta_1 u - 2u^* v, \\ iv_z &= -\frac{1}{2}v_{xx} + (\beta_2 - q)v - u^2. \end{aligned} \tag{4}$$

Our main goal is the analysis of the effect of the interplay between nonconservative terms and coupling between the two systems of solitons governed by (1). For the analysis of stationary solutions, we first define the total energy flow in the j-th waveguide $P_j = \int(|u_j|^2 + 2|v_j|^2)dx$. In the conservative case ($\gamma_1 = \gamma_2 = 0$), the total energy $P = P_1 + P_2$, is constant along propagation. In the presence of the gain and loss, it is generally not so anymore, and one computes

$$\frac{dP}{dz} = 2\gamma_1\int(|u_1|^2 - |u_2|^2)dx + 4\gamma_2\int(|v_1|^2 - |v_2|^2)dx. \tag{5}$$

This relation means that for a *stationary* solution, i.e., the solution of the form $u_j = \tilde{u}_j(x)e^{i\beta z}$ and $v_j = \tilde{v}_j(x)e^{2i\beta z}$, the difference in the energy flows is defined by

$$P_1 - P_2 = (1 - \gamma_1/\gamma_2)\int(|u_1|^2 - |u_2|^2)dx. \tag{6}$$

Thus, if $\gamma_1 \neq \gamma_2$ (what corresponds to the most typical situation) the equality of the energy flows in two different waveguides requires $|u_1| = |u_2|$ and $|v_1| = |v_2|$. Further, we notice that due to the $\mathcal{PT}$ symmetry, if a column-vector $\psi = (u_1(x, z), v_1(x, z), u_2(x, z), v_2(x, z))^T$ is a solution of (1), then the $\mathcal{PT}$-transformed field $\tilde{\psi} = \mathcal{PT}\psi = (u_2^*(x, -z), v_2^*(x, -z), u_1^*(x, -z), v_1^*(x, -z))^T$ is also a solution. Thus, a stationary $\mathcal{PT}$-symmetric solution, which is defined by the relation $\mathcal{PT}\psi = \psi$ (or, more generally, $\mathcal{PT}\psi = e^{i\vartheta}\psi$, where ϑ is a constant phase) supports the equality of the power flows. On the other hand, if, for a given solution $P_1 \neq P_2$, then the obtained solution is non-$\mathcal{PT}$-symmetric.

A large diversity of the particular solutions of the system (4) can be found [6]. To restrict the number of cases, below we concentrate on the simplest ones and start with the $\mathcal{PT}$-symmetric solutions. Using the well-known [3] soliton of (4), we obtain that such $\mathcal{PT}$-symmetric soliton exists subject to the constraint (3), when $\gamma_1 = \kappa_1\sin(\delta)$ and $\gamma_2 = \kappa_2\sin(2\delta)$

$$\begin{aligned} u_1 &= 3\beta^2 e^{ipz}/\cosh^2(\beta x), \qquad u_2 = \pm u_1 e^{\mp i\delta}, \\ v_1 &= 3\beta^2 e^{2ipz}/\cosh^2(\beta x), \qquad v_2 = \pm v_1 e^{\mp 2i\delta}, \end{aligned} \tag{7}$$

where

$$p = \frac{1}{3}[2q + \kappa_1\cos(\delta) - 2\kappa_2\cos(2\delta)], \tag{8}$$

$$\beta^2 = \frac{1}{6}[q + 2\kappa_1\cos(\delta) - \kappa_2\cos(2\delta)]. \tag{9}$$

The right-hand side of the last equation must be positive, which imposes the constraint on the mismatch of the propagation constants: $q > q_0(\delta) = \kappa_2\cos(2\delta) - 2\kappa_1\cos(\delta)$. For the conservative case $\delta = 0$, we have that $q_0(\delta = 0) = q_{\text{cons}} = \kappa_2 - 2\kappa_1$. Furthermore, one can verify that $q_0(\delta) < q_{\text{cons}}$ for the interval $\delta \in (0, \pi/2)$, i.e., the gain and loss introduced in the system reduce the lower band for q for which the exact solution (7) exists; see inset (a) of Fig. 2 for an illustration. For all other δ (i.e., for $\delta \in (\pi/2, \pi)$), one has that $q_0 > q_{\text{cons}}$.

The numerical stability analysis was performed by studying the evolution of initially perturbed stationary states according to (1) along z and investigating signals of instability. The perturbation is invoked at $z = 0$ by multiplying the initial conditions for each component of the vector ψ introduced above by the factor $(1 + 10^{-3}n_j)$, with $j = 1, 2, 3, 4$ and n_j being uncorrelated Gaussian random numbers with zero mean and unit

variance. We then first evaluated to monitor several different signals of instability for threshold values of 10% deviation from the initial values during the evolution $0 < z \le z_m = 10$ for each of the four moduli of the fields. We numerically found different quantities (and components) to perform qualitatively similar with respect to determining instability. These quantities were the center of mass, the (maximum) amplitude, and the root mean square (RMS) width. Therefore, for transparency, the results on stability presented here (Fig. 2) are based on only one signal of instability (for only the first component u_1), that is, the RMS width. If no signal of instability occurred, we repeated the analysis with $z_m = 10^2$. All calculations were done with the C^{++} code generator XMDS [21,22].

Our main numerical results on the stability of solutions are summarized in Fig. 2. In the main panel, we show the stability of conservative solitons on the diagram (q, κ_2) for $\kappa_1 = 1$. The solitons exist above the dashed line, which corresponds to the exact analytical solution, i.e., described by (7) with $q = q_{\rm cons}$ and $\delta = 0$. The solitons in the green stripe above the dashed line were found stable. All other solitons with a larger mismatch of propagation constants are unstable (red domain).

Turning now to the stability of $\mathcal{PT}$-symmetric solitons given by (7)–(9) with the gain and loss fulfilling the relation (3) in the general case ($0 \le \gamma_1 < \kappa_1 = 1$ and $0 \le \gamma_2 < \kappa_2$), we show the stability analysis in the two diagrams (γ_1, γ_2) [insets in Fig. 2] for different sets of the "conservative" parameters. The gain and loss can stabilize solitons, see inset (b) of Fig. 2, where we show a branch of solutions in the plane (γ_1, γ_2), which bifurcates from an (arbitrarily chosen) unstable conservative soliton marked by a blue cross in the main panel. Hence, we observe that a sufficiently large gain and loss can stabilize the solutions (computed stable solitons are shown by green dots). Furthermore, since the domain of existence of localized solutions in the presence of the gain and loss is larger than that of the conservative case, we considered stability of solitons which do not exist in the conservative limit. An illustrative example is shown in inset (a) of Fig. 2 and corresponds to the set of parameters indicated by the asterisk on the main panel. We again

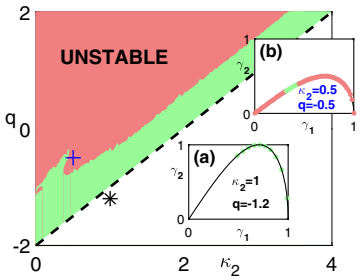

Fig. 2. Stability for solitons (7) with equal intensity profiles of the FF and SHs. The main panel shows the conservative case ($\gamma_1 = \gamma_2 = 0$). The inset plots are for the specific values of κ_2 and q, where $0 \le \gamma_1 < \kappa_1 = 1$ and $0 \le \gamma_2 < \kappa_2$ are given by (3). The dashed diagonal line in the main figure is $q_{\rm cons}$, discussed under (9). Inset (b) shows how an unstable solution in the conservative case, marked by a blue cross on the main panel, can be stabilized by the loss and gain (the green domain for $0.32 \lesssim \gamma_1 \lesssim 0.45$). Inset (a) shows examples of a branch of solutions for $0.49 \le \gamma_1 \le 0.99$ situated below $q_{\rm cons}$, at the (black) asterisk in the main panel. The (red) green dots in the insets are for (un-) stable solutions (up to $z_m = 10^2$). The step size in the numerics was $dz = 10^{-3}$, and the transverse domain $|x| < 50$ ($dx = 0.1$). The resolution in the main panel was $\Delta\kappa_2 = \Delta q = 0.02$.

observed that, at a sufficiently large gain and loss, there exists a stability window (green dots).

Such solitons can be observed in a system of tunnel-coupled slab waveguides of $LiNbO_3$ [8,23] of a characteristic length ~5 cm. For an input beam width ~60 μm, the diffraction length is $L_d \approx 2.0$ mm, corresponding to $z \approx 25$. A typical linear coupling length is $L_c = \pi/K_j \approx (1 - 2)$ cm, corresponding to $\kappa_1 \approx \kappa_2 \approx (0.1–0.2)$. The absorption and gain induced by active impurity doping can vary in the range $\lesssim 0.17(0.35)$ dB cm^{-1} for the FF (SHs), i.e., $\gamma_1 \approx 0.05, \gamma_2 \approx 0.1$ in the dimensionless variables. Experimentally, feasible input powers for soliton generation for quadratic nonlinearity parameter $\chi^{(2)} = 5.6$ pm/V are ~10 kW, corresponding to $u \sim 1$ (dimensionless).

Stable $\mathcal{PT}$-symmetric solitons were tested with respect to the mutual interactions; an example is shown in Fig. 3, and we verified that the energy is constant ($P_1 = P_2 = $ constant) when (3) is fulfilled. The collision, however, cannot be seen as strictly elastic, because weak modulation of the pulse shapes after the collision is detectable.

In the case of the SHs generation in a single waveguide, an approximate solution can be obtained in the so-called cascading limit, which corresponds to the large mismatch parameter $|q| \gg 1$ [11]. This allows one to reduce the description of the two component systems to the single nonlinear Schrödinger equation for the FF only. A similar reduction is also possible in the case of the $\mathcal{PT}$-symmetric coupler (1). To this end, we introduce $\Delta = q^2 + \gamma_2^2 - \kappa_2^2$ and require $|\Delta|$ to be large enough. Notice that this last condition can be satisfied not only due to a large mismatch q (as in the conservative systems), but also due to the strong coupling κ_2 of the SHs. Now the derivatives of $v_{1,2}$ can be neglected and one computes

$$v_1 \approx -\frac{(q + i\gamma_2)u_1^2 + \kappa_2 u_2^2}{\Delta}, \quad v_2 \approx -\frac{(q - i\gamma_2)u_2^2 + \kappa_2 u_1^2}{\Delta}. \tag{10}$$

The equations for the FF are now reduced to

$$iu_{1,z} = -u_{1,xx} + \kappa_1 u_2 + i\gamma_1 u_1 + \frac{2(q + i\gamma_2)}{\Delta}|u_1|^2 u_1 + \frac{2\kappa_2}{\Delta}u_1^* u_2^2,$$
$$iu_{2,z} = -u_{2,xx} + \kappa_1 u_1 - i\gamma_1 u_2 + \frac{2(q - i\gamma_2)}{\Delta}|u_2|^2 u_2 + \frac{2\kappa_2}{\Delta}u_2^* u_1^2. \tag{11}$$

Thus, we obtained a $\mathcal{PT}$-symmetric coupler with self-phase modulation and the four-wave mixing terms due to coupling of the SHs, as well as with linear and nonlinear gain and loss. At $\gamma_2 = 0$, (11) is reduced to the $\mathcal{PT}$-symmetric dimer model [20,24] while, for an x-independent plane wave solution (11),

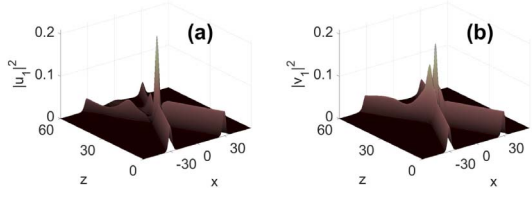

Fig. 3. Interaction of two solitons with equal intensity profiles of the FF and SHs, given by (7). Panel (a)/(b) shows the modulus square of the u_1 - /v_1-component. From (7), we see that $|u_2|^2$ and $|v_2|^2$ are proportional to those. The parameters here were $\kappa_1 = 1$, $\kappa_2 = 0.5$, $q = -1$, $\gamma_1 = 0.5$, and $\gamma_2 \simeq 0.433$, i.e., from (3), with a velocity of $w = \pm 1$ for the two initial pulses.

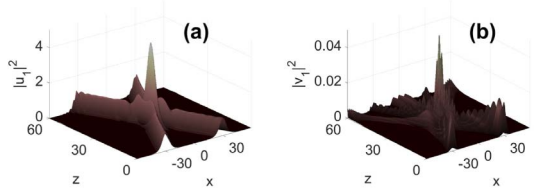

Fig. 4. Interaction of two solitons with initial profiles obtained from the cascading limit (10) and (12). The parameters for the initial conditions here were $A = 1$, $\kappa_1 = 1$, $\kappa_2 = 20$, $q = -3$, and $\gamma_1 = \gamma_2 = 0.1$ (i.e., $\Delta \simeq -400$), and $w = \pm 1$.

becomes the nonlinear coupler [25]. Both limits have been studied in the literature (see e.g., [15] and references therein). The gain and loss in the second component, thus, introduce nonlinear the gain and loss for the first component. An interesting feature of the cascading limit (11) is that the sign of its effective Kerr-like nonlinearity is determined by the coefficient q/Δ and, hence, can be either focusing ($q/\Delta < 0$) or defocusing ($q/\Delta > 0$). A soliton solution of (11) is readily found:

$$u_1 = A\,\mathrm{sech}\left(Ax/\sqrt{\kappa_2\cos(2\delta) - q}\right), \quad u_2 = \pm u_1 e^{\mp i\delta}, \qquad (12)$$

provided the condition (3) holds and the additional constraint $q < \kappa_2 \cos(2\delta)$ is satisfied. After having numerically confirmed the stability of the approximate solutions (10) and (12) (given that $|\Delta| \gg 1$ and small $\gamma_{1,2}$), we have also tested those solutions with respect to mutual interactions; see Fig. 4 for an example. We have verified that we have solitons for a large domain of initial conditions fulfilling $|\Delta| \gg 1$ though, generally, with oscillating energies P_1 and P_2 in the two waveguides (with $P_1 + P_2 \neq$ constant), unless the condition (3) is fulfilled.

To quantify how (10) and (12) works for different values of Δ, we define the following numerical measure:

$$\langle \Delta X^2 \rangle_{z_m} \equiv \langle |X^2(z) - X^2(0)| \rangle_{z_m} / X^2(0), \qquad (13)$$

where $\langle f \rangle_{z_m} = z_m^{-1} \int_0^{z_m} f(z)\mathrm{d}z$ with $X^2(z) = P_1^{-1} \int x^2 (|u_1|^2 + 2|v_1|^2)\mathrm{d}x$. Here z_m should be chosen large enough such that $\langle \Delta X^2 \rangle_{z_m}$ is qualitatively independent of z_m. The characterization of the solutions using the parameter $\langle \Delta X^2 \rangle_{z_m}$ is shown in Fig. 5, where we used $z_m = 10^4$ ($dz = 10^{-3}$) and $|x| < 10^2$ ($dx = 0.2$) for all curves. We observe that for the parameter Δ, in spite of the fact that it is composed of three system

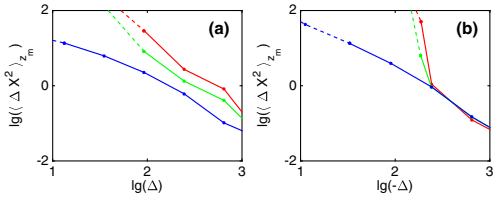

Fig. 5. Characterization of the solutions in the cascading limit, using (10) and (12) for the initial conditions. In (a), ($\Delta > 0$) q was varied, while $\kappa_2 = 1$ ($\kappa_1 = 1$). In (b), ($\Delta < 0$) κ_2 was varied, while $q = 1$. The blue curves are for $\gamma_1 = \gamma_2 = 0$, and the red curves are for $\gamma_1 = \gamma_2 = 0.05$. The green curve in (a) is for $\gamma_1 = 0.05$ and $\gamma_2 \simeq 0.0999$, according to Eq. (3). When varying κ_2 ($\Delta < 0$), the use of Eq. (3) leads to different values of γ_2; the resulting green curve in (b) is partly overlapping the red. For the data points with dashed curves to the left, a drift along x was notable.

parameters (due to (3), only two of them are independent), the curves for different q and κ_2 indicate the same qualitative behavior in the cascading limit, and that the average deformation of the soliton shape (13) decreases fast with $|\Delta|$. This numerically confirms the validity of the approach.

To conclude, we have obtained two families of stable $\mathcal{PT}$-symmetric solitons in a $\mathcal{PT}$-symmetric $\chi^{(2)}$ coupler. We numerically found, in the case of solitons with equal shapes of the first and second harmonics, a region of stability for the solitons. It is established that the gain and loss can increase the domain of soliton existence with respect to the propagation constant mismatch and can stabilize solitons which are unstable in the conservative limit. Stable solitons interact nearly elastically. We also analyzed the cascading limit, which is reduced to a $\mathcal{PT}$-symmetric dimer with the linear and nonlinear gain and loss. The solitons in this limit can still be found stable, but their interactions manifest appreciable non-elastic effects.

Funding. International Islamic University Malaysia (IIUM) (FRGS 16-014-0513).

Acknowledgment. V. Konotop acknowledges the hospitality of Örebro University (Sweden) and IIUM.

REFERENCES

1. C. Etrich, F. Lederer, B. A. Malomed, T. Peschel, and U. Peschel, Prog. Opt. **41**, 483 (2000).
2. A. V. Buryak, P. Di Trapani, D. V. Skryabin, and S. Trillo, Phys. Rep. **370**, 63 (2002).
3. Y. N. Karamzin and A. P. Sukhorukov, Sov. Phys. JETP. **41**, 414 (1976).
4. M. J. Werner and P. D. Drummond, Opt. Lett. **19**, 613 (1994).
5. M. J. Werner and P. D. Drummond, J. Opt. Soc. Am. B **10**, 2390 (1993).
6. C. R. Menyuk, R. Schiek, and L. Torner, J. Opt. Soc. Am. B **11**, 2434 (1994).
7. A. V. Buryak and Y. S. Kivshar, Opt. Lett. **19**, 1612 (1994).
8. R. Schiek, Y. Baek, and G. Stegeman, Phys. Rev. E **53**, 1138 (1996).
9. R. Schiek, Y. Baek, G. Stegeman, and W. Sohler, Opt. Lett. **24**, 83 (1999).
10. R. Iwanow, R. Schiek, G. Stegeman, T. Pertsch, F. Lederer, Y. Min, and W. Sohler, Opto-Electron. Rev. **13**, 113 (2005).
11. G. I. Stegeman, D. J. Hagan, and L. Torner, Opt. Quantum Electron. **28**, 1691 (1996).
12. M. A. Karpierz, Opt. Appl. **26**, 391 (1996).
13. W. C. K. Mak, B. A. Malomed, and P. L. Chu, Phys. Rev. E **55**, 6134 (1997).
14. C. M. Bender, Rep. Prog. Phys. **70**, 947 (2007).
15. V. V. Konotop, J. Yang, and D. A. Zezyulin, Rev. Mod. Phys. **88**, 035002 (2016).
16. D. A. Antonosyan, A. S. Solntsev, and A. A. Sukhorukov, Opt. Lett. **40**, 4575 (2015).
17. R. El-Ganainy, J. I. Dadap, and R. M. Osgood, Opt. Lett. **40**, 5086 (2015).
18. T. Wasak, P. Szańkowski, V. V. Konotop, and M. Trippenbach, Opt. Lett. **40**, 5291 (2015).
19. K. Li, D. A. Zezyulin, P. G. Kevrekidis, V. V. Konotop, and F. Kh. Abdullaev, Phys. Rev. A **88**, 053820 (2013).
20. R. Driben and B. A. Malomed, Opt. Lett. **36**, 4323 (2011).
21. G. R. Collecutt and P. D. Drummond, Comput. Phys. Commun. **142**, 219 (2001).
22. G. R. Dennis, J. J. Hope, and M. T. Johnsson, Comput. Phys. Commun. **184**, 201 (2013).
23. R. Schiek, Y. Baek, G. Krijnen, G. I. Stegeman, I. Baumann, and W. Sohler, Opt. Lett. **21**, 940 (1996).
24. F. Kh. Abdullaev, V. V. Konotop, M. Ögren, and M. P. Sørensen, Opt. Lett. **36**, 4566 (2011).
25. A. E. Miroshnichenko, B. A. Malomed, and Y. S. Kivshar, Phys. Rev. A **84**, 012123 (2011).